Canadian Science Publishing
NRC Research Press journals | Publishing Services

Biochemistry and Cell Biology
Biochimie et biologie cellulaire

The Quinone-Binding Site of Acidithiobacillus ferrooxidans Sulfide:Quinone Oxidoreductase Controls both Sulfide Oxidation and Quinone Reduction

Journal:	*Biochemistry and Cell Biology*
Manuscript ID	bcb-2015-0097.R1
Manuscript Type:	Article
Date Submitted by the Author:	27-Nov-2015
Complete List of Authors:	Zhang, Yanfei; University of Alberta, Department of Biochemistry Qadri, Ali; University of Alberta, Department of Biochemistry Weiner, Joel; University of Alberta,
Keyword:	Quinone reduction, quinone inhibitors, midpoint potential, binding affinity

The Quinone-Binding Site of *Acidithiobacillus ferrooxidans* Sulfide:Quinone Oxidoreductase Controls both Sulfide Oxidation and Quinone Reduction

Yanfei Zhang, Ali Qadri and Joel H. Weiner*

Membrane Protein Disease Research Group, Department of Biochemistry, University of Alberta, Edmonton, Alberta T6G 2H7, Canada

*Corresponding author: Joel H. Weiner

Department of Biochemistry,

University of Alberta,

Edmonton, Alberta T6G 2H7, Canada

Phone office: +1 780-492-2761

Phone lab: +1 780-492-2558

Fax: +1 780-492-0886

Email: joel.weiner@ualberta.ca

Abstract

Sulfide:quinone oxidoreductase (SQR) is a peripheral membrane enzyme that catalyzes the oxidation of sulfide and the reduction of ubiquinone. Ubiquinone binds to a conserved hydrophobic domain and shuttles electrons from a non-covalent FAD cofactor to the membrane-bound quinone pool. Utilizing the structure of decylubiquinone bound to *Acidithiobacillus ferrooxidans* SQR, we combined site-directed mutagenesis and kinetic approaches to analyze quinone binding. SQR can reduce both benzoquinones and naphthoquinones. The alkyl side chain of ubiquinone derivatives enhances binding to SQR but limits the enzyme turnover. Pentachlorophenol and 2-*n*-heptyl-4-hydroxyquinoline-*N*-oxide are potent inhibitors of SQR with apparent inhibition constants (K_i) of 0.46 μM and 0.58 μM, respectively. The highly conserved amino acids surrounding the quinone binding site play an important role in quinone reduction. The phenyl sidechains of Phe357 and Phe391 sandwich the benzoquinone head group and are critical for quinone binding. Importantly, conserved amino acids that define the ubiquinone-binding site also play an important role in sulfide oxidation/flavin reduction.

Keywords: Quinone reduction; quinone inhibitors; midpoint potential; binding affinity

Introduction

Sulfide (existing as three different forms: H_2S, HS^- and S^{2-})[1] is involved in a variety of biological processes. In mammals, it is considered a very toxic molecule, which inhibits mitochondrial ATP production (Cooper and Brown 2008). Recently sulfide has been identified as a signaling molecule and plays prominent roles in cellular physiology and pathophysiology, including the regulation of vascular homeostasis, inflammation, apoptosis, and cellular stress response (Li et al. 2011; Szabo 2007; Wallace and Wang 2015; Wang 2002). However, it can be used as an energy source by microbes, such as the acidophilic chemolithotrophic bacterium *Acidithiobacillus ferrooxidans* (Shahak and Hauska 2008; Temple and Delchamps 1953; Zhang et al. 2013).

A key enzyme in maintaining the sulfide homeostasis is sulfide:quinone oxidoreductase (SQR)[2], an ancient flavoprotein that is present in all domains of life (although it is absent in the plant kingdom). SQR is a peripheral membrane protein and catalyzes the oxidation of sulfide species to elemental sulfur by transferring two electrons from a sulfide ion via the FAD cofactor to the quinone pool in the membrane. In SQR, three conserved Cys residues (Cys128, Cys160 and Cys356) in close proximity to the FAD are proposed to play key roles in sulfide oxidation through a nucleophilic attack mechanism or a radical mechanism (Cherney et al. 2012; Cherney et al. 2010; Zhang and Weiner 2014). SQR interacts with the membrane via two amphipathic helices and the quinone-pool through a conserved hydrophobic domain (Cherney et al. 2010). Quinones, the most important lipophilic electron and proton carriers, can undertake $2e^-/2H^+$ oxidation-reduction reactions and shuttle electrons and protons between respiratory enzymes via the membrane-bound quinone pool. Different types of natural quinones, comprising mainly benzoquinones, naphthoquinones, anthraquinones and polycyclic quinones, are widely distributed in different organisms. Animals and plants use ubiquinones (1,4-benzoquinones or *p*-benzoquinone) in their mitochondrial membrane quinone-pool, while bacteria use a mixture of quinones including ubiquinones, naphthoquinones and the derivatives menaquinone and rhodoquinone for bioenergetic reactions. The distribution in the redox potentials ($E_{m,7}$) of

[1] In this paper the term "sulfide" will refer to the total sulfide present in solution including the three different forms: H_2S, HS^- and S^{2-}. The species H_2S, SH^- and S^{2-} will be named specifically as necessary.

[2] *Abbreviations:* SQR, sulfide:quinone oxidoreductase; DUQ, decylubiquinone; ANSO, Anthraquinone sulfonate; DHBQ, 2,5-Dihydroxy-1,4-benzoquinone; TTFA, Thenoyltrifluoroacetone; HOQNO, 2-*n*-heptyl 4-hydroxyquinoline-*N*-oxide; PCP, Pentachlorophenol

quinones and the derivatives ranges from ~ -400 mV for the non-physiological anthraquinones to ~ +110 mV for the physiological ubiquinones (Clark 1960). A significant shift of the redox potential can be caused by hydroxylation or methylation on the quinone motif. e.g. duroquinone ($E_{m,7}$ = +7 mV), menadione ($E_{m,7}$ = -12 mV), lawsone ($E_{m,7}$ = -119 mV) and plumbagin ($E_{m,7}$ = -40 mV) (Ratasuk and Nanny 2007).

In SQR the site of quinone binding has been determined from the co-crystallized $SQR_{At,f}$-decylubiquinone (DUQ) complex structure (Cherney et al. 2010). The binding site of decylubiquinone (DUQ) is confined to the hydrophobic region that is close to the two C-terminal amphipathic helices (α9 and α10, residues 321-427). The benzoquinone ring of DUQ is sandwiched between the two benzene rings of Phe357 and Phe394 with the center-to-center distance of 3.4 Å and 3.8 Å respectively (**Fig. 1**). Out of a total of 47 atom-atom interactions with DUQ within a distance of 3.9 Å, 24 are made to these two phenylalanine residues (**Table S1**). The other interacting residues Phe41, Pro43, Gly322, Tyr323, Asn353, Ile368, Lys391 and Tyr411, together with Phe357 and Phe394, form a hydrophobic pocket (**Fig. 1**). The benzoquinone head is also located close to the isoalloxazine ring of FAD; the distance between the O2 atom of the quinone and the O2 atom of FAD is less than 3 Å (**Fig. 1c**). The hydrophobic quinone tail (decyl chain) points away from the amphipathic helices. It interacts with the protein via the side chains of Tyr323, Asn353, Ile368, and Tyr411, which are located at the entrance of the hydrophobic pocket. Sequence conservation analysis indicated that these four amino acids are not conserved. However, of the ten residues interacting with the DUQ, the other six (Phe41, Pro43, Gly322, Phe357, Phe394 and Lys391) interacting with the headgroup of DUQ are highly conserved and potentially necessary for either structural integrity and/or biological activity (**Fig. S1**).

In this study we have examined the quinone-binding site using quinone analogues and quinone site inhibitors. Site-directed mutagenesis combined with pre-steady state and steady state kinetics have been applied to wild-type SQR and variants of amino acids comprising the quinone binding site. Our results show that the quinone-binding site also plays an important role in sulfide oxidation.

Materials and Methods

Bacterial Strains and Plasmids

E. coli strain DH10B (F^- *end*A1 *rec*A1 *gal*E15 *gal*K16 *nup*G *rps*L Δ*lac*X74 Φ80*lac*ZΔM15 *ara*D139 Δ(*ara,leu*)7697 *mcr*A Δ(*mrr-hsd*RMS-*mcr*BC) λ^-; Invitrogen) was used for mutagenesis. *E. coli* BL21(DE3) (F^- *omp*T *gal dcm lon hsd*S_B(r_B^- m_B^-) λ(DE3 [*lac*I *lac*UV5-T7 gene 1 *ind*1 *sam*7 *nin*5])) was used for all enzyme expression. Wild-type SQR was expressed from plasmid pLM1::SQR under the control of the T7 promoter (Zhang et al. 2009).

Quinones, Quinone analogs and Inhibitors

Decylubiquinone (DUQ), ubiquinone Q0 (UQ0), 2,3,5,6-tetramethylcyclohexa-2,5-diene-1,4-dione (Duroquinone), 2,5-dihydroxy-1,4-benzoquinone (DHBQ), 1,4-naphthoquinone (NQ), 2-hydroxy-1,4-naphthoquinone (Lawsone), 5-hydroxy-1,4-naphthoquinone (Juglone), anthraquinone-2-sulfonic acid sodium salt monohydrate (ANSO), 5-hydroxy-2-methyl-1,4-naphthoquinone (Plumbagin), 2-methyl-1,4-naphthoquinone (Menadione), pentachlorophenol (PCP), 4,4,4-trifluoro-1-(2-thienyl)-1,3-butanedione (TTFA), 6-methyl-N-phenyl-2,3-dihydro-1,4-oxathiine-5-carboxamide (Carboxin) and antimycin A were obtained from Sigma–Aldrich (St Louis, MO). 2-*n*-heptyl 4-hydroxyquinoline-*N*-oxide (HOQNO) was purchased from Alexis Biochemicals (San Diego, CA).

Site-directed Mutagenesis of Quinone site Mutants

Construction of the site-directed variants was carried out following the QuikChange method (Stratagene) using pLM1::SQR plasmid as the template for mutagenesis (Zhang et al. 2009; Zhang and Weiner 2014). The oligonucleotides used are listed in **Table S2** and were obtained from Integrated DNA Technologies (Coraville, IA). All recombinant plasmids were verified by DNA sequencing (DNA core facility, University of Alberta).

Enzyme Expression and Purification

Enzyme expression and purification was performed as previously described (Zhang et al. 2009). The protein fractions were buffer-exchanged (to remove imidazole) and concentrated to 5 mg/mL in buffer (50 mM MOPS, 0.5 M NaCl, pH 7.0) using a YM-30 Centricon tube (Amicon) as soon as possible after the purification and flash-frozen as

aliquots with liquid N_2 before being stored at -80°C prior to use (Zhang and Weiner 2014). All steps of protein purification were performed at 4°C.

Protein Assays

Protein concentrations were determined by the Bradford method with bovine serum albumin as the standard (Bradford 1976). Ten µg of purified wild-type and variants were analyzed by 12% SDS-polyacrylamide gel electrophoresis (SDS-PAGE) (Laemmli 1970). Low-molecular-mass markers were obtained from Bio-Rad. Gel electrophoresis was run at 200 V for 45 min, and the gel was stained with Coomassie Brilliant Blue.

Measurement of Enzyme Activity

The quinone reduction activity of SQR was measured as described previously (Zhang and Weiner 2014). Measurements were carried out with a Hewlett Packard 8453 UV-VIS diode array spectrophotometer at 23°C. The standard reaction mixture contained 50 mM Bis-Tris (pH 7.0) and 20 mM glucose. To establish anoxic conditions, the 50 mM Bis–Tris (pH 7.0) and 20 mM glucose were first mixed and flushed with N_2; 1 unit of glucose oxidase per mL and 10 units of catalase per mL were added to the assay medium when needed. The reaction was started by the addition of 100 µM freshly prepared Na_2S. The sulfide-decylubiquinone (DUQ) reduction activity of SQR was measured in the presence of varying concentrations of DUQ. The reaction was followed by the decrease of absorbance at 275 nm (ε_{275}= 12.5 mM^{-1} cm^{-1}) as described previously (Morton 1965; Shahak et al. 1994). The sulfide-UQ_0 reduction activity was determined in the presence of varying concentrations of UQ_0 (ε_{275}= 12 mM^{-1} cm^{-1}). The sulfide-duroquinone reduction activity was determined by the decrease of absorbance at 275 nm (ε_{275}= 12.5 mM^{-1} cm^{-1}) in the presence of varying concentrations of duroquinone. The sulfide-DHBQ reduction activity was monitored by following the loss of absorbance at 340 nm (ε_{340}= 2.89 mM^{-1} cm^{-1}) (Sirdeshmukh et al. 2006). The sulfide-naphthoquinone reduction activity was determined in the presence of varying concentrations of 1,4-naphthoquinone (ε_{265}= 4.01 mM^{-1} cm^{-1}), lawsone (ε_{275}= 15.17 mM^{-1} cm^{-1}), juglone (ε_{420}= 1.96 mM^{-1} cm^{-1}), plumbagin (ε_{275}= 10.3 mM^{-1} cm^{-1}) or menadione (ε_{275}= 2.38 mM^{-1} cm^{-1}), respectively. The rates of photo reduction of quinones and quinone analogs were measured and subtracted in all of the assays.

Determination of Kinetic Constants

V_{max} and Michaelis constant (K_m) for Na_2S, DUQ and quinone analogs were determined by nonlinear fitting of the Michaelis-Menten equation using GraphPad Prism (GraphPad Software, San Diego, CA). Measurements were carried out using the quinone reduction activity assay method as described above at 23°C. One mL anoxic reaction mixture contained 1.25 μg/mL wild-type SQR (or 12.5 μg/mL or 25 μg/mL SQR variant) and varying concentration of Na_2S at constant DUQ (50 μM) or varying concentration of quinone or quinone analog at constant Na_2S (100 μM). The k_{cat} was calculated based on the specific activity, molecular weight of SQR and the amount of protein used in the assay.

Inhibition of SQR

The half maximal inhibitory concentration (IC_{50}) for selected inhibitors was determined at varying concentrations of the inhibitors at a constant concentration of DUQ (50 μM) in the quinone reduction activity assay described above. All inhibitor stock solutions were prepared in ethanol. The final concentration of ethanol did not exceed 1.5 % (v/v) in the assays. The IC_{50} values were determined by plotting residual enzyme activity against drug concentrations and extrapolated graphically. The *in vitro* inhibition constants (K_i) were calculated assuming a competitive inhibition model and applying the Cheng-Prusoff equation for competitive inhibition (K_i=IC_{50}/(S/K_m+1) (Brandt et al. 1987), where substrate concentration [S] is 50 μM, Michaelis-Menten constant K_m is 3.43 μM.

Stopped-flow spectrophotometry and enzymatic activity assay based on the reduction of FAD

Stopped-flow experiments were performed at 23°C using an Applied Photophysics SX.18MV stopped-flow instrument equipped with a multiwavelength photodiode array (PDA) detector and X-SCAN software (Applied Photophysics Ltd, Leatherhead, UK). The optical path length was 1 cm. The dead time of the apparatus was 1.28 ms. The buffer (50 mM Bis-Tris, 20 mM glucose, 3 U mL^{-1} glucose oxidase and 10 units of catalase per mL, pH 7.0) and SQR in the same buffer were degassed with repeated cycles of vacuum and flushing with N_2. Na_2S was freshly dissolved and diluted in the degassed buffer before loading to the sample syringes. The flow system was flushed thoroughly with the anaerobic buffer prior to the experiments.

The FAD reduction assay was performed in the absence of DUQ by monitoring the reduction of FAD after rapidly mixing SQR (25 μM after mixing) with freshly prepared

sulfide (125 μM after mixing) in 50 mM Bis-Tris buffer (pH 7.0) containing 20 mM glucose, 3 unit of glucose oxidase per mL and 10 units of catalase per mL. The buffer was degassed with repeated cycles of vacuum and flushing with N_2. Stopped-flow mixing chambers were washed with the deoxygenated buffer to establish the anoxic conditions. The reaction was monitored in the stopped-flow by multiwavelength absorption in the range of 300−700 nm. Temporal changes in absorbance at 448 nm were fitted to the double exponential equation (two-phase exponential decay equation) $\text{Abs} = \square_1\square^{-\square\text{Fast}\square} + \square_2\square^{-\square\text{Slow}\square} + \square$ or the one-phase exponential decay equation $\text{Abs} = \square_1\square^{-\square\square} + \square$ with GraphPad Prism (GraphPad Software, San Diego, CA), where A_1 and A_2 are amplitudes, k_{Fast} and k_{Slow} (k for a one-phase decay) are the rate constants describing the observed rate at which the dependent variable is decreasing, expressed in s^{-1}, t is time, and b is the end point of the data trace. The rate constants k_{Fast} (for the two-phase decay) or k (for the one-phase decay) obtained from fitting was used to indicate the FAD reduction activity.

Redox Potentiometry and Electron paramagnetic resonance (EPR) spectroscopy

Redox titrations were carried out anaerobically under argon at 25 °C on wild-type SQR and the $\text{SQR}^{\text{Phe357Ala/Phe394Ala}}$ variant at a total protein concentration of 50 μM in 50 mM MOPS, 0.5 M NaCl, pH 7.0. The following redox mediators (dyes) were used at a concentration of 25 μM: quinhydrone (+287 mV), 2,6-dichlorophenolindolphenol (+217 mV), 1,2-naphthoquinone (+125 mV), toluylene blue (+115 mV), phenazine methosulfate (+80 mV), thionine (+60 mV), methylene blue (−11 mV), resorufin (−50 mV), indigo trisulfonate (−80 mV), indigo carmine (−125 mV), anthraquinone-2-sulfonic acid (−225 mV), phenosafranine (−255 mV), and neutral red (−329 mV). All samples were prepared in 3-mm internal diameter quartz EPR tubes, rapidly frozen in liquid nitrogen-chilled ethanol, and stored in liquid nitrogen until analyzed. EPR spectra were recorded using a Bruker Elexsys E500 spectrometer equipped with a Bruker liquid nitrogen-evaporating cryostat at 150 K, 20-milliwatt microwave power at 9.43 GHz. All spectra reported are the average of five scans using the modulation amplitude of 4.0 G_{pp} at 100 KHz modulation frequency. Potentiometric titration data were analyzed by plotting the signal height of peak-trough amplitude versus E_h (electrode potential relative to the standard hydrogen half cell) and fitting the data to two midpoint potential values (E_{m1} and E_{m2}) using the equation $[SQ] = C_{\text{site}}[(1+10^{(E_h-E_{m1})/59}+10^{(E_{m2}-E_h)/59})]^{-1}$ (Hastings et al. 1998); where C_{site} is the concentration of

binding sites (assumed to equal the concentration of SQR), E_h is the electrode potential relative to the standard hydrogen half cell, E_{m1} is defined as the potential of the quinone/semiquinone couple, and E_{m2} as the potential of the semiquinone/quinol couple. The highest radical signal would then be observed at E_m, the midpoint potential value of the E_{m1}/E_{m2} couple [$E_m = 0.5(E_{m1} + E_{m2})$]. E_m values were representative of two (WT) and three ($SQR^{Phe357Ala/Phe394Ala}$) independent titrations with a S.D. value of ± 5 mV.

Results

SQR can use both benzoquinones and naphthoquinones as electron acceptors.

SQR catalyzes the oxidation of sulfide and the reduction of ubiquinone via a non-covalent FAD cofactor. In previous publications we have utilized decylubiquinone as an artificial electron acceptor to monitor catalytic activity (Zhang and Weiner 2014). Additionally, a crystal structure of decylubiquinone bound in the quinone site has been published (Cherney et al. 2010). Herein we measured the efficiency of several quinone analogues to serve as an electron acceptor for Na_2S oxidation by determining k_{cat}/K_m at steady state. As shown in **Table 1**, SQR was able to use benzoquinones and naphthoquinones but not water soluble anthraquinone sulfonate. All of the analogues except DUQ (K_m 3.4 ± 0.4 μM) had very high K_m values varying from 26.0 ± 6.0 μM for 5-hydroxy-1,4 naphthoquinone to 193 ± 15.6 μM for UQ_0. UQ_0 and 1,4-naphthoquinone had the highest k_{cat} values but DUQ was the most efficient acceptor with a k_{cat}/K_m of 2.2 $\mu M^{-1}s^{-1}$ due to its low K_m although it had a low k_{cat} of 7.6 ± 0.2 s^{-1}. All the other quinones had much lower k_{cat}/K_m values in the undetectable to 0.4 $\mu M^{-1}s^{-1}$ range. There was no obvious correlation between redox potential, K_m or k_{cat} although acceptors with higher redox potentials were somewhat better.

Quinone inhibitors of SQR

Five well-studied quinone inhibitors were tested for their inhibitory potency on SQR activity: pentachlorophenol (PCP), 2-(n-heptyl-4-hydroxyquinolone N-oxide (HOQNO), theonyltrifluoroactone (TTFA), carboxin and antimycin A. The half maximal inhibitory concentrations (IC_{50}) were determined and the *in vitro* inhibition constants (K_i) were then calculated using the Cheng-Prusoff equation (**Table 2**). PCP and HOQNO were

effective inhibitors with IC_{50} values are 7.1 ± 1.8 μM and 9.1 ± 1.6 μM, respectively. Their apparent inhibition constants (K_i) were 0.46 μM and 0.58 μM, respectively. In contrast, TTFA, carboxin and antimycin A showed weak inhibition with the IC_{50} values of 200 ± 9 μM, 260 ± 11 μM and 350 ± 25 μM, respectively. The apparent inhibition constants (K_i) were 13 μM, 17 μM and 22 μM, respectively.

Kinetic analysis of the variants involved in quinone binding and reduction in SQR

The quinone binding pocket of SQR comprises six conserved amino acids. Two Phe residues (Phe357 and Phe394) sandwich the benzoquinone ring and Phe41, Pro43, Gly322, and Lys391 interact with the ring. Tyr323, Asn353, Ile368 and Tyr411 interact with the hydrophobic isoprenoid side chain of the quinone but are not highly conserved. To investigate the role of each of these amino acids in quinone binding and SQR catalysis, variants were constructed and characterized by pre-steady state and steady state kinetic assays. For each variant the enzyme was expressed, and contained the FAD cofactor in approximately 0.7:1 molar ratio similar to the wild-type (Zhang and Weiner 2014). The wild-type and each variant enzyme was purified by FPLC Ni-affinity chromatography prior to enzymatic analysis. Two kinetic assays were used to characterize the variants. A pre-steady state reaction follows the Na_2S dependent reduction of FAD (**Fig. 2 and Fig. S2)** and a Na_2S dependent reduction of DUQ measures the overall catalytic activity of the variants (**Table 3 and Fig. S3)**.

Phe357 and Phe394 sandwich the benzoquinone ring

The benzoquinone ring of the DUQ is sandwiched between the aromatic rings of Phe357 and Phe394 (Cherney et al. 2010). Phe357 is situated next to one of the essential cysteines (Cys356) and interacts with the O4 atom of FAD through its main-chain nitrogen and oxygen atoms at a distance of 3.42 Å and 3.18 Å, respectively (Cherney et al. 2010). In contrast, Phe394 is ~7 Å away from FAD. Alanine variants were generated at these positions to verify that the hydrophobic "sandwiching" of the benzoquinone head group is critical for activity. Both variants retained less than 10% wild-type steady-state activity with k_{cat} values of 0.3 ± 0.01 s^{-1} and 0.6 ± 0.02 s^{-1}, respectively (**Table 3**). Surprisingly, for the $SQR^{Phe357Ala}$ variant the K_m for DUQ was not altered but the K_m for Na_2S increased 13-

fold (40.8 ± 3.5 μM). The SQR^{Phe394Ala} variant also had an unaltered K_m for DUQ and the K_m for Na_2S showed a slight increase (8.05 ± 2.8 μM). When both Phe residues were converted to Ala the enzyme was totally inactive. We also attempted to examine the Na_2S dependent pre-steady state reduction of FAD in the SQR^{Phe357Ala}, SQR^{Phe394Ala} and SQR$^{Phe357Ala/Phe394Ala}$ variant enzymes but no FAD bleaching was detectable beyond FAD photoreduction of 0.1 ± 0.05 s^{-1} (Zhang and Weiner 2014) (**Fig. 2**). To examine if alteration of these Phe residues affects the redox potential of FAD in SQR, potentiometric titrations of the FAD semiquinone of the wild-type SQR and SQR$^{Phe357Ala/Phe394Ala}$ variant were performed at neutral pH (**Fig. 3**). Curve fitting of the FAD semiquinone signal revealed a midpoint potential of -136 ± 5 mV (E_{m1} = -71 ± 5 mV, E_{m2} = -200 ± 5 mV) at pH 7.0 in SQR$^{Phe357Ala/Phe394Ala}$ variant, which is similar to that in wild-type SQR (E_m = -139 ± 5 mV; E_{m1} = -58 ± 5 mV, E_{m2} = -220 ± 5 mV).

Phe41, Pro43, Gly322 and Lys391 encompass the quinone binding pocket

Phe41, Pro43 and Gly322 were substituted with Ala and Lys391 was substituted with Ala, Asp, Glu and Arg. In the steady state assay, SQR^{Phe41Ala} and SQR^{Pro43Ala} variants retained about 15% activity with k_{cat} values of 1.2 ± 0.04 s^{-1} and 1.3 ± 0.03 s^{-1}, respectively and Michaelis constants for Na_2S and DUQ similar to the wild-type enzyme. However, the SQR^{Gly322Ala} variant was expressed and assembled but was totally inactive (**Table 3**) indicating that placing a side chain in this position was highly disruptive to catalysis.

In the pre-steady state kinetic assay, the SQR^{Phe41Ala} variant retained about 75% of FAD reduction activity (**Fig. S3**) with an observed rate constant (k_{Fast}) of 8.8 ± 1.8 s^{-1}. In contrast, the SQR^{Pro43Ala} and SQR^{Gly322Ala} variants exhibited very slight activity (k_{Fast}) of 0.15±.01 s^{-1} and 0.12±.01 s^{-1} respectively, slightly above FAD photoreduction (0.1 ± 0.05 s^{-1}) (Zhang and Weiner 2014).

Lys391 is located within hydrogen-bonding distance of both DUQ and FAD in SQR. Its side chain ζ-amine group could interact with the C-4 keto oxygen (the O4 atom) of FAD and/or of DUQ, and participate in proton transfer (**Table S1 and S3**). In order to identify the function of Lys391, Ala, Glu, Asp and Arg variants were generated. The SQR^{Lys391Ala}, SQR^{Lys391Asp} and SQR^{Lys391Glu} variants were totally inactive in both the pre-steady state and steady state kinetic assays (**Fig. 2 and Table 3**). In contrast, the SQR^{Lys391Arg} variant

retained 62.5% of FAD reduction activity in the pre-steady state kinetic assay (**Fig. 2** and **Fig. S2**), but only ~1% DUQ reductase activity with a k_{cat} value of 0.1 ± 0.01 s^{-1} (**Table 3 and Fig. S3**). Overall this suggests that Lys391 participates primarily in quinone reduction.

Tyr323, Asn353, Ile368 and Tyr411 interact with the hydrophobic quinone tail

Tyr323, Asn353, Ile368 and Tyr411 are situated around the entrance of the quinone binding pocket in SQR and are not highly conserved. Based on our crystal structure of DUQ bound to SQR (PDB ID: 3T31), all interact with the hydrophobic quinone tail (Cherney et al. 2010). To examine the catalytic role of these residues, each was substituted with Ala. Additionally Tyr411 was converted to Phe.

In the steady state kinetic assay, mutation of these residues resulted in almost complete loss of activity with k_{cat} values of 0.2 to 0.9 s^{-1}, corresponding to 3-13% of the activity of wild-type SQR (**Table 3**). When we examined the pre-steady state kinetics of FAD reduction, only the $SQR^{Asn353Ala}$ and $SQR^{Tyr411Phe}$ variants retained measurable rates corresponding to 53.8% and 91.2% of wild-type with k_{Fast} of 6.3 ± 0.3 s^{-1} and 10.7 ± 2.4 s^{-1}, respectively. This suggests that Asn353 and Tyr411 are not involved in FAD reduction but play a role in $FADH_2$ oxidation even though they are distant from the ubiquinone head group as part of the quinone tail hydrophobic binding domain. Variants of Tyr323, Ile368 (and Tyr411Ala) eliminated sulfide oxidation/flavin reduction either due to coupling between the Cys-sulfide-flavin and quinone sites or due to conformational changes.

Discussion

Acidithiobacillus ferrooxidans SQR couples the oxidation of sulfides such as H_2S, HS^- and S^{2-} to the reduction of ubiquinone via a non-covalent FAD cofactor with an $E_{m,7}$ (FAD) of -139 mV (Zhang and Weiner 2014). SQR is relatively small and the three-dimensional structure of SQR indicates that the quinone binding site is very close to the FAD which in turn is close to the catalytic sulfide oxidation site consisting of Cys160, Cys356 and FAD. Thus one could predict that mutations of conserved amino acids in the quinone binding site could have profound effects not only on quinone reduction but also on sulfide oxidation and sulfide mediated FAD reduction.

Inspection of structurally characterized quinone sites in many dehydrogenases and reductases does not provide a well-defined structural binding motif but some general features can be discerned (Fisher and Rich 2000; Rich 1996). Quinone-binding sites are hydrophobic and normally have several aromatic residues (Phe, Tyr, His or Trp) within 4 Å of the quinone molecule. In the quinone site of SQR three aromatic residues (Phe41, Phe357 and Phe394) interact with the quinone ring and an additional two aromatic residues (Tyr323 and Tyr411) interact with the quinone tail. We investigated the role of the quinone binding site in SQR catalysis and showed that the enzyme could use both benzoquinones and naphthoquinones and that there was no obvious correlation between K_m or k_{cat} and activity although there was a rough correlation between the redox potential ($E_{m,7}$) of quinone and activity (*i.e.* quinones with a more positive $E_{m,7}$ than -139 mV exhibited greater activity).

At.f SQR was inhibited by PCP and HOQNO. These inhibitors have been shown to bind to the quinone binding site of nitrate reductase, succinate dehydrogenase and fumarate reductase (Bertero et al. 2005; Maklashina and Cecchini 1999). The apparent IC_{50} value of HOQNO (9.1 µM) for $SQR_{At.f}$ is close to that for SQRs from *Aquifex aeolicus* and *Rhodobacter capsulatus* (12 µM and 5.6 µM, respectively) (Nubel et al. 2000; Shahak et al. 1994). Interestingly, antimycin A, a strong inhibitor of the SQRs from *Aquifex aeolicus*, *Paracoccus denitrificans* and *Rhodobacter capsulatus* with the apparent IC_{50} values of 10 µM, 15 µM and 50 µM, respectively (Nubel et al. 2000; Schutz et al. 1998; Shahak et al. 1994) was inactive towards *At.f* SQR.

We employed a site-directed mutagenesis approach of the quinone binding site to create variants of residues that interact with the benzoquinone ring and hydrophobic tail of the quinone and subjected the variant enzymes to steady state kinetic analysis of Na_2S dependent reduction of DUQ and pre-steady state kinetic analysis of Na_2S-dependent flavin reduction.

Conversion of either of the two Phe residues (Phe357 and Phe394) that sandwich the benzoquinone ring to Ala resulted in no affect on the midpoint potential of FAD in SQR, but a 90% loss of DUQ activity. In these variants we could not observe Na_2S-dependent flavin bleaching. This suggests that mutation of these Phe residues also results in conformational changes at the catalytic Na_2S oxidation site consisting of Cys160, Cys356 and FAD. However we cannot rule out that very limited residual activity might result from flavin-independent direct DUQ reduction by Na_2S within the enzyme. This is supported by the lack of FAD bleaching and the increased K_m of Na_2S in the variants.

Four additional conserved amino acids are found within the quinone binding site. Mutation of Phe41 to Ala had minimal effect on FAD reduction but reduced the overall reaction rate by 85%. Given that Phe41 is 6.5 Å from the FAD this is not unexpected. Mutation of Pro43 or Gly322 to Ala reduced both FAD and DUQ reduction to very low levels. As these two amino acids are within 4 Å of both FAD and DUQ, this indicates close conformational coupling between the sulfide oxidation site and the quinone site. As noted above we cannot rule out direct Na_2S reduction of DUQ in the enzyme. Lys391 hydrogen bonds to both the quinone (backbone amide) and FAD (N_ζ). Mutation to Arg had only a small effect on FAD reduction/sulfide oxidation but eliminated DUQ reduction. Mutation to Ala, or acidic residues Asp or Glu eliminated both FAD and DUQ reduction. Thus mutation to another positive amino acid was tolerated for the FAD reduction/sulfide oxidation step but not DUQ reduction. Placing a neutral or acidic residue in this position was not tolerated.

Tyr323, Asn353, Ile368 and Tyr411 make up the isoprenoid binding channel for the quinone and interact with the DUQ decyl chain. Mutation of any of these amino acids to Ala eliminated DUQ reduction. A similar perturbation of the isoprenoid binding channel has been observed in SQR from the archaea *Caldivirga maquilingensis* (Lencina et al. 2013). Mutation of Tyr323, Ile368 or Tyr411 to Ala also eliminated Na_2S reduction of

FAD. This was unexpected as these residues are physically distant from the FAD and Na_2S catalytic site. Mutation of Asn353 to Ala or Tyr411 to Phe retained significant FAD reduction activity.

The two ketone oxygens (O1 and O4) of oxidized quinone are hydrogen bond acceptors. The typical hydrogen bond partners include the polar/ionizable residues Glu, Asp, Lys; the polar residues His, Ser, Tyr, Arg, backbone NH and water molecules (Zheng et al. 2010). In SQR, a Tyr (Tyr411) is located within hydrogen-bonding distance of the DUQ C-1 ketone oxygen (O1); the distance between the O1 atom of DUQ and the OH of Y411 is 3.4 Å (**Table S1 and Fig. S2**). The conserved Lys391 has a long flexible side-chain with a positively-charged amine that could be more inclined to interact with the FAD C-4 carbonyl oxygen within a distance of 3.6 Å. The distance between N_ζ atom of Lys391 and the O4 atom of DUQ is 4.5 Å. The hydrogen bonding between Lys391 and DUQ may need the assistance of a water molecule or a rotation of the side-chain of Lys391. Such interactions are commonplace in the quinone sites of enzymes such as *Escherichia coli* menaquinol:fumarate and menaquinol:nitrate oxidoreductases (Bertero et al. 2005; Maklashina et al. 2006; Rothery et al. 2005). The backbone nitrogen of Gly322 is distant from the DUQ ketone group (>5 Å), but is able to hydrogen bond to the FAD C-2 carbonyl oxygen within a distance of 2.4 Å.

The quinone site of *Aquifex aeolicus* SQR is the only other structurally characterized SQR quinone site (Marcia et al. 2009). *At.f* SQR has 40% sequence identity with *Aq. aeolicus* SQR. The superposition of the *At.f* SQR structure with the structure of *Aq. aeolicus* SQR (PDB ID: 3HYW) shows high similarity with a root-mean-square deviation (RMSD) value of about 1.3 Å for 401 C_α atoms (**Fig. 4**). Both of the quinone sites are located in the hydrophobic region and close to the isoalloxazine ring of FAD. The amino acids (Phe41, Pro43, Lys391 and Phe394; in the *At. ferrooxidans* numbering) interacting with the benzoquinone head are similar except that the aromatic ring is bound between the benzene ring of Phe385 and the side chain of Ile346 in *Aq. aeolicus* SQR. In contrast, the amino acids that interact with the hydrophobic quinone tail are varied due to the high flexibility of the amphipathic helices in the C-terminal domain (**Fig. 3**).

Overall our kinetic analysis shows that there is an intimate conformational connection between the catalytic Na_2S oxidation site and the quinone reduction site; and shed new light on the understanding of the quinone site of *At. ferrooxidans* SQR.

Acknowledgements.

The authors thank Justin G. Fedor and Dr. Richard A. Rothery for reviewing this manuscript and helpful discussions. This work was funded by the Canadian Institutes of Health Research (CIHR MOP89735).

Reference

Bertero, M.G., Rothery, R.A., Boroumand, N., Palak, M., Blasco, F., Ginet, N., Weiner, J.H., and Strynadka, N.C. 2005. Structural and biochemical characterization of a quinol binding site of *Escherichia coli* nitrate reductase A. The Journal of biological chemistry **280**(15): 14836-14843. doi: 10.1074/jbc.M410457200.

Bradford, M.M. 1976. A rapid and sensitive method for the quantitation of microgram quantities of protein utilizing the principle of protein-dye binding. Anal Biochem **72**: 248-254. doi: S0003269776699996 [pii].

Brandt, R.B., Laux, J.E., and Yates, S.W. 1987. Calculation of inhibitor Ki and inhibitor type from the concentration of inhibitor for 50% inhibition for Michaelis-Menten enzymes. Biochemical medicine and metabolic biology **37**(3): 344-349.

Cherney, M.M., Zhang, Y., James, M.N., and Weiner, J.H. 2012. Structure-activity characterization of sulfide:quinone oxidoreductase variants. Journal of structural biology **178**(3): 319-328. doi: 10.1016/j.jsb.2012.04.007.

Cherney, M.M., Zhang, Y., Solomonson, M., Weiner, J.H., and James, M.N.G. 2010. Crystal structure of sulfide:quinone oxidoreductase from *Acidithiobacillus ferrooxidans*: insights into sulfidotrophic respiration and detoxification. J Mol Biol **398**(2): 292-305. doi: 10.1016/j.jmb.2010.03.018.

Clark, W.M. 1960. Oxidation-reduction potentials of organic systems. Williams and Wilkins Co, Baltimore.

Cooper, C.E., and Brown, G.C. 2008. The inhibition of mitochondrial cytochrome oxidase by the gases carbon monoxide, nitric oxide, hydrogen cyanide and hydrogen sulfide: chemical mechanism and physiological significance. Journal of bioenergetics and biomembranes **40**(5): 533-539. doi: 10.1007/s10863-008-9166-6.

Fisher, N., and Rich, P.R. 2000. A motif for quinone binding sites in respiratory and photosynthetic systems. Journal of Molecular Biology **296**(4): 1153-1162. doi: Doi 10.1006/Jmbi.2000.3509.

Hastings, S.F., Kaysser, T.M., Jiang, F., Salerno, J.C., Gennis, R.B., and Ingledew, W.J. 1998. Identification of a stable semiquinone intermediate in the purified and membrane bound ubiquinol oxidase-cytochrome bd from Escherichia coli. European journal of biochemistry / FEBS **255**(1): 317-323.

Laemmli, U.K. 1970. Cleavage of structural proteins during the assembly of the head of bacteriophage T4. Nature **227**(5259): 680-685.

Lencina, A.M., Ding, Z., Schurig-Briccio, L.A., and Gennis, R.B. 2013. Characterization of the Type III sulfide:quinone oxidoreductase from Caldivirga maquilingensis and its membrane binding. Biochimica et biophysica acta **1827**(3): 266-275. doi: 10.1016/j.bbabio.2012.10.010.

Li, L., Rose, P., and Moore, P.K. 2011. Hydrogen sulfide and cell signaling. Annual review of pharmacology and toxicology **51**: 169-187. doi: 10.1146/annurev-pharmtox-010510-100505.

Maklashina, E., and Cecchini, G. 1999. Comparison of catalytic activity and inhibitors of quinone reactions of succinate dehydrogenase (Succinate-ubiquinone oxidoreductase) and fumarate reductase (Menaquinol-fumarate oxidoreductase) from *Escherichia coli*. Archives of biochemistry and biophysics **369**(2): 223-232. doi: 10.1006/abbi.1999.1359.

Maklashina, E., Hellwig, P., Rothery, R.A., Kotlyar, V., Sher, Y., Weiner, J.H., and Cecchini, G. 2006. Differences in protonation of ubiquinone and menaquinone in fumarate reductase from *Escherichia coli*. The Journal of biological chemistry **281**(36): 26655-26664. doi: 10.1074/jbc.M602938200.

Marcia, M., Ermler, U., Peng, G., and Michel, H. 2009. The structure of *Aquifex aeolicus* sulfide: quinone oxidoreductase, a basis to understand sulfide detoxification and respiration. Proceedings of the National Academy of Sciences **106**(24): 9625-9630.

Morton, R.A. 1965. Spectroscopy of quinones and related substances. Academic Press Inc, London. pp. 23-64.

Nubel, T., Klughammer, C., Huber, R., Hauska, G., and Schutz, M. 2000. Sulfide:quinone oxidoreductase in membranes of the hyperthermophilic bacterium Aquifex aeolicus (VF5). Arch Microbiol **173**(4): 233-244.

Ratasuk, N., and Nanny, M.A. 2007. Characterization and quantification of reversible redox sites in humic substances. Environmental science & technology **41**(22): 7844-7850.

Rich, P.R. 1996. Quinone binding sites of membrane proteins as targets for inhibitors. Pestic Sci **47**(3): 287-296.

Rothery, R.A., Seime, A.M., Spiers, A.M., Maklashina, E., Schroder, I., Gunsalus, R.P., Cecchini, G., and Weiner, J.H. 2005. Defining the Q-site of *Escherichia coli* fumarate reductase by site-directed mutagenesis, fluorescence quench titrations and EPR spectroscopy. The FEBS journal **272**(2): 313-326. doi: 10.1111/j.1742-4658.2004.04469.x.

Schutz, M., Klughammer, C., Griesbeck, C., Quentmeier, A., Friedrich, C.G., and Hauska, G. 1998. Sulfide-quinone reductase activity in membranes of the chemotrophic bacterium Paracoccus denitrificans GB17. Arch Microbiol **170**(5): 353-360.

Shahak, Y., and Hauska, G. 2008. Sulfide oxidation from cyanobacteria to humans: Sulfide–Quinone Oxidoreductase (SQR). Sulfur Metabolism in Phototrophic Organisms: 319-335.

Shahak, Y., Klughammer, C., Schreiber, U., Padan, E., Herrman, I., and Hauska, G. 1994. Sulfide-quinone and sulfide-cytochrome reduction in *Rhodobacter capsulatus*. Photosynthesis Research **39**(2): 175-181.

Sirdeshmukh, D.B., Sirdeshmukh, L., and Subhadra, K.G. 2006. Micro- and macro-properties of solids thermal, mechanical and dielectric properties. *In* Springer series in materials science,. Springer-Verlag, Berlin. pp. xvii, 403 p.

Szabo, C. 2007. Hydrogen sulphide and its therapeutic potential. Nature reviews. Drug discovery **6**(11): 917-935. doi: 10.1038/nrd2425.

Temple, K.L., and Delchamps, E.W. 1953. Autotrophic bacteria and the formation of acid in bituminous coal mines. Applied microbiology **1**(5): 255-258.

Wallace, J.L., and Wang, R. 2015. Hydrogen sulfide-based therapeutics: exploiting a unique but ubiquitous gasotransmitter. Nat Rev Drug Discov **14**(5): 329-345. doi: 10.1038/nrd4433.

Wang, R. 2002. Two's company, three's a crowd: can H2S be the third endogenous gaseous transmitter? The FASEB journal : official publication of the Federation of American Societies for Experimental Biology **16**(13): 1792-1798. doi: 10.1096/fj.02-0211hyp.

Zhang, Y., Cherney, M.M., Solomonson, M., Liu, J., James, M.N., and Weiner, J.H. 2009. Preliminary X-ray crystallographic analysis of sulfide:quinone oxidoreductase from Acidithiobacillus ferrooxidans. Acta crystallographica. Section F, Structural biology and crystallization communications **65**(Pt 8): 839-842. doi: 10.1107/S1744309109027535.

Zhang, Y., and Weiner, J.H. 2014. Characterization of the kinetics and electron paramagnetic resonance spectroscopic properties of Acidithiobacillus ferrooxidans sulfide:quinone oxidoreductase (SQR). Archives of biochemistry and biophysics **564**: 110-119. doi: 10.1016/j.abb.2014.09.016.

Zhang, Y.F., Yang, Y., Liu, J.S., and Qiu, G.Z. 2013. Isolation and characterization of *Acidithiobacillus ferrooxidans* strain QXS-1 capable of unusual ferrous iron and sulfur utilization. Hydrometallurgy **136**: 51-57. doi: Doi 10.1016/J.Hydromet.2013.03.005.

Zheng, Z., Dutton, P.L., and Gunner, M. 2010. The measured and calculated affinity of methyl - and methoxy - substituted benzoquinones for the QA site of bacterial reaction centers. Proteins: Structure, Function, and Bioinformatics **78**(12): 2638-2654.

Figure Legends.

Fig. 1 The quinone binding site of *At. ferrooxidans* SQR (PDB ID: 3T31). The highly conserved amino acids surrounding the quinone site are shown as sticks in the cartoon representation (a) and labeled in surface representation (b). DUQ and FAD (yellow) are shown as sticks in Fig. (a) and (b); (c) The 2D sketch of the SQR-DUQ-FAD complex was generated using the online software tool PoseView (http://poseview.zbh.uni-hamburg.de).

Fig. 2 The relative rate constants (k_{Fast}) of SQR and variants in pre-steady state reduction of FAD by Na_2S. 100% of the k_{Fast} is 11.71 ± 0.97 s^{-1}. Insert is the apparent rate constants (k_{Fast}) of SQR and variants in pre-steady state reduction of FAD by Na_2S. The data are the mean values of three experiments; error bars indicate the standard deviation.

Fig. 3 Potentiometric titration of the FAD radical signal in wild-type SQR (a) and $SQR^{Phe357Ala/Phe394Ala}$ variant (b) at pH 7.0. Peak-trough differentials were plotted as a function of E_h. Signal heights are normalized to 100%. Presented data were gathered from two independent potentiometric titrations for both wild-type and variant enzyme.

Fig. 4 Superposition of the structures of the quinone binding sites of *At. ferrooxidans* SQR (green, PDB ID: 3T31) and *Aquifex aeolicus* SQR (magenta, PDB ID: 3HYW). The atoms of the FAD cofactors (yellow) were used for this superposition. DUQ and the amino acids surrounding the quinone binding sites are represented by sticks. The amino acids are labeled in black (for *At. ferrooxidans* SQR) and in red (for *Aquifex aeolicus* SQR) respectively.

Tables.

Table 1 Redox potential and steady-state kinetic parameters of SQR with quinone homologues and analogs

Name	Rings	Redox Potential ($E_{m,7}$= mV)	K_m (μM)	k_{cat} (s^{-1})	k_{cat}/K_m ($\mu M^{-1}\ s^{-1}$)
Decylubiquinone (DUQ)	1	~ +110	3.4 ± 0.4	7.6 ± 0.2	2.2
Ubiquinone-0 (UQ0)	1	+100	193.0 ± 15.6	47.7 ± 4.7	0.2
Tetramethyl-1,4-benzoquinone (Duroquinone)	1	+7	31.4 ± 3.4	11.3 ± 0.9	0.4
2,5-Dihydroxy-1,4-benzoquinone (DHBQ)	1	-60	n.d.	0.0	n.d
1,4-Naphthoquinone (NQ)	2	+60	76.9 ± 7.1	33.8 ± 2.2	0.4
2-Methyl-1,4-naphthoquinone (Menadione)	2	-12	71.6 ± 11.9	19.5 ± 2.6	0.3
2-Hydroxy-1,4-naphthoquinone (Lawsone)	2	-139	72.1 ± 13.6	1.2 ± 0.3	0.0
5-Hydroxy-1,4-naphthoquinone (Juglone)	2	+33	26.0 ± 6.1	6.3 ± 1.4	0.2
5-Hydroxy-2-methyl-1,4-naphthoquinone (Plumbagin)	2	-40	44.7 ± 5.3	3.4 ± 0.3	0.1
Anthraquinone sulfonate (ANSO)	3	-225	n.d.	n.d.	n.d.

n.d. : not determined

Table 2 Inhibition of SQR activity.

Name	IC_{50} (μM)	K_i * (μM)
Pentachlorophenol (PCP)	7.1 ± 1.8	0.46
2-(n-heptyl)-4-hydroxyquinoline N-oxide (HOQNO)	9.1 ± 1.6	0.58
Thenoyltrifluoroacetone (TTFA)	200 ± 9	12.84
Carboxin	260 ± 11	16.69
Antimycin A	350 ± 25	22.47

* Apparent inhibition constant values (K_i) were calculated using the Cheng-Prusoff equation ($Ki = IC_{50} / (1+[S]/K_m)$), where substrate (DUQ) concentration [S] = 50 μM. Michaelis constant K_m = 3.4 μM.

Table 3 Steady-state kinetic parameters of wild-type SQR and variants

Variant	k_{cat} (s^{-1})	K_m[Na_2S] (μM)	K_m[DUQ] (μM)	k_{cat}/K_m[Na_2S] ($\times 10^6$ $M^{-1}s^{-1}$)	k_{cat}/K_m[DUQ] ($\times 10^6$ $M^{-1}s^{-1}$)
SQR	7.6 ± 0.2	3.0 ± 0.3	3.4 ± 0.4	2.55	2.20
F41A	1.2 ± 0.04	4.8 ± 1.2	2.1 ± 0.5	0.25	0.59
P43A	1.3 ± 0.03	2.7 ± 0.6	2.9 ± 0.4	0.48	0.44
G322A	0.0	n.d.	n.d.	n.d.	n.d.
Y323A	0.2 ± 0.01	2.2 ± 0.7	2.3 ± 0.5	0.09	0.09
N353A	0.5 ± 0.03	3.4 ± 0.7	13.9 ± 3.0	0.15	0.04
F357A	0.3 ± 0.01	40.8 ± 3.5	3.6 ± 0.5	0.01	0.08
I368A	0.4 ± 0.02	8.1 ± 2.5	4.9 ± 1.3	0.05	0.07
K391A	0.0	n.d.	n.d.	n.d.	n.d.
K391D	0.0	n.d.	n.d.	n.d.	n.d.
K391E	0.0	n.d.	n.d.	n.d.	n.d.
K391R	0.1 ± 0.01	7.3 ± 2.5	2.4 ± 0.7	0.01	0.03
F394A	0.6 ± 0.02	7.5 ± 1.3	3.5 ± 0.4	0.08	0.18
Y411A	0.6 ± 0.02	2.8 ± 1.0	3.8 ± 0.8	0.20	0.15
Y411F	0.9 ± 0.07	42.4 ± 2.4	13.1 ± 3.3	0.02	0.07
F357A/F394A	0.0	n.d.	n.d.	n.d.	n.d.

n.d. : not determined

Figures

Fig. 1

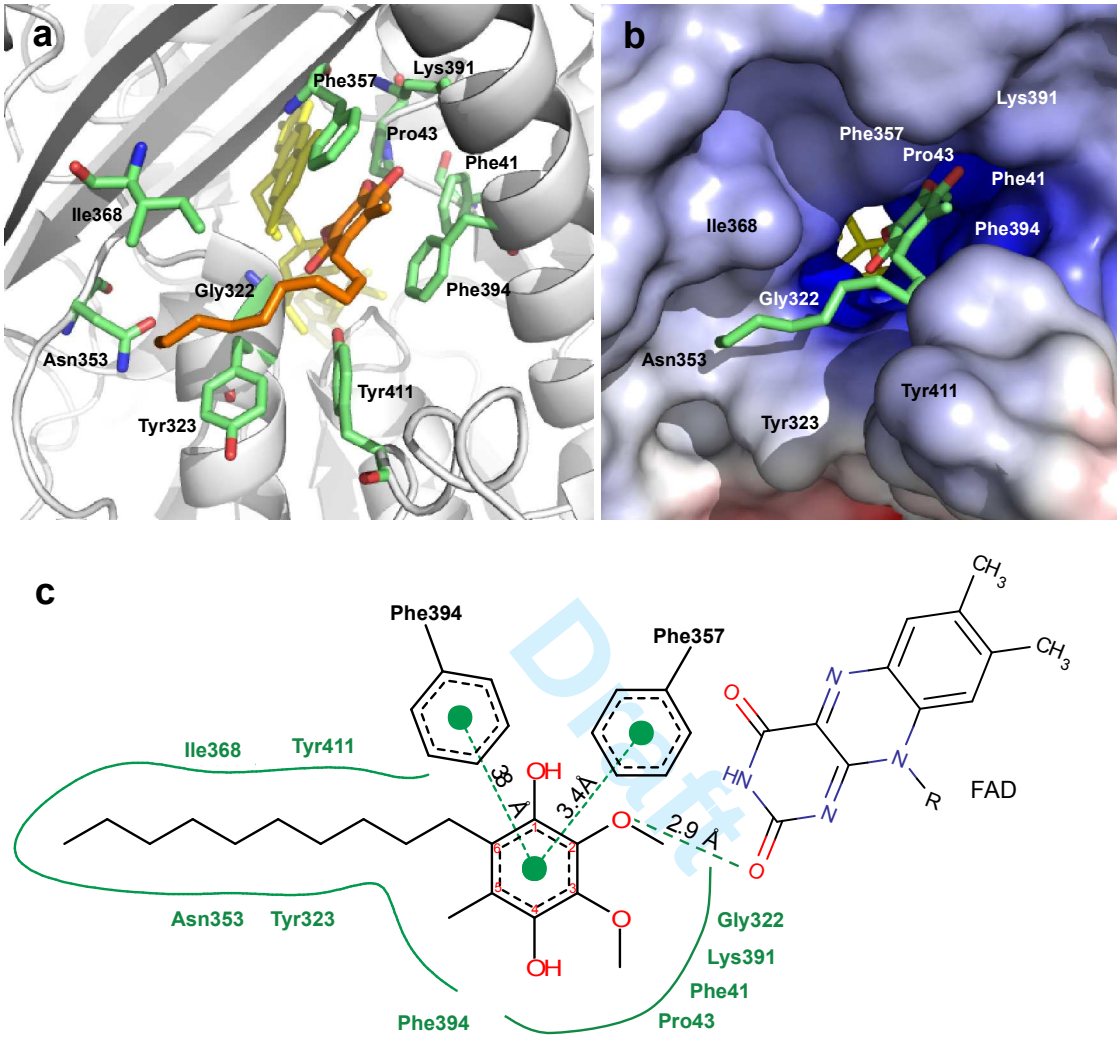

Fig. 2

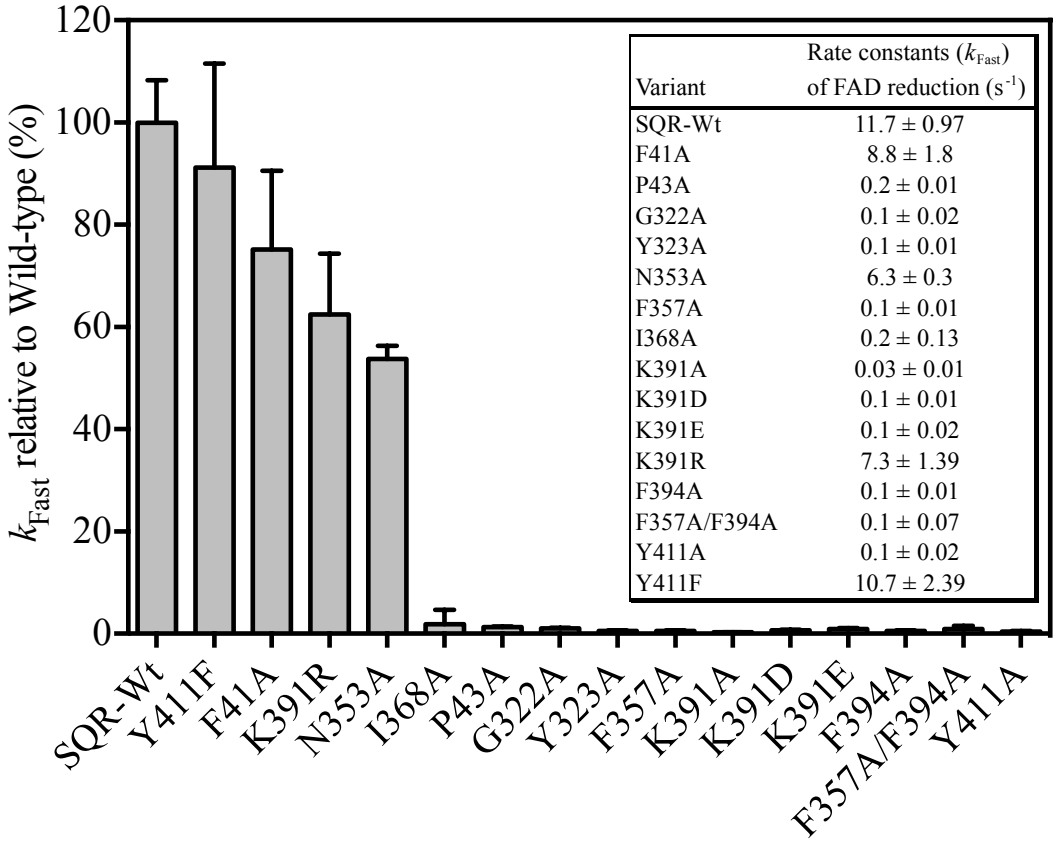

Variant	Rate constants (k_{Fast}) of FAD reduction (s^{-1})
SQR-Wt	11.7 ± 0.97
F41A	8.8 ± 1.8
P43A	0.2 ± 0.01
G322A	0.1 ± 0.02
Y323A	0.1 ± 0.01
N353A	6.3 ± 0.3
F357A	0.1 ± 0.01
I368A	0.2 ± 0.13
K391A	0.03 ± 0.01
K391D	0.1 ± 0.01
K391E	0.1 ± 0.02
K391R	7.3 ± 1.39
F394A	0.1 ± 0.01
F357A/F394A	0.1 ± 0.07
Y411A	0.1 ± 0.02
Y411F	10.7 ± 2.39

Fig. 3

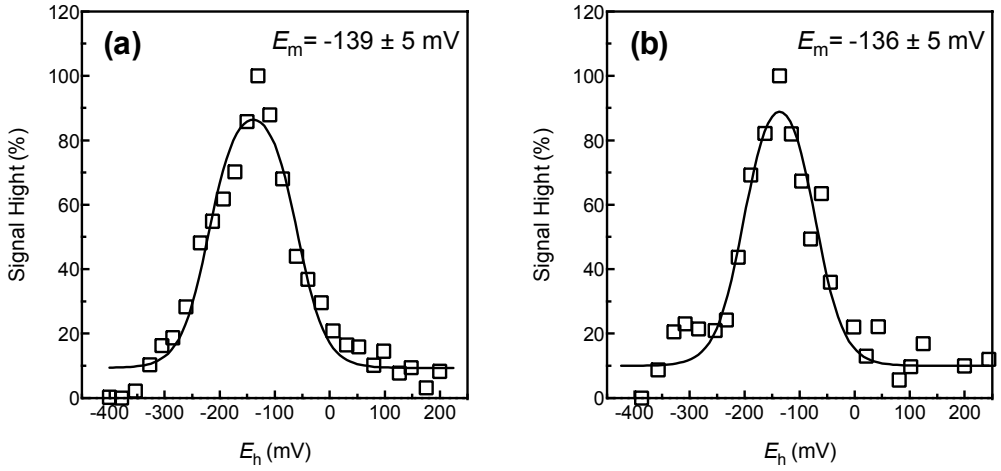

Fig. 4

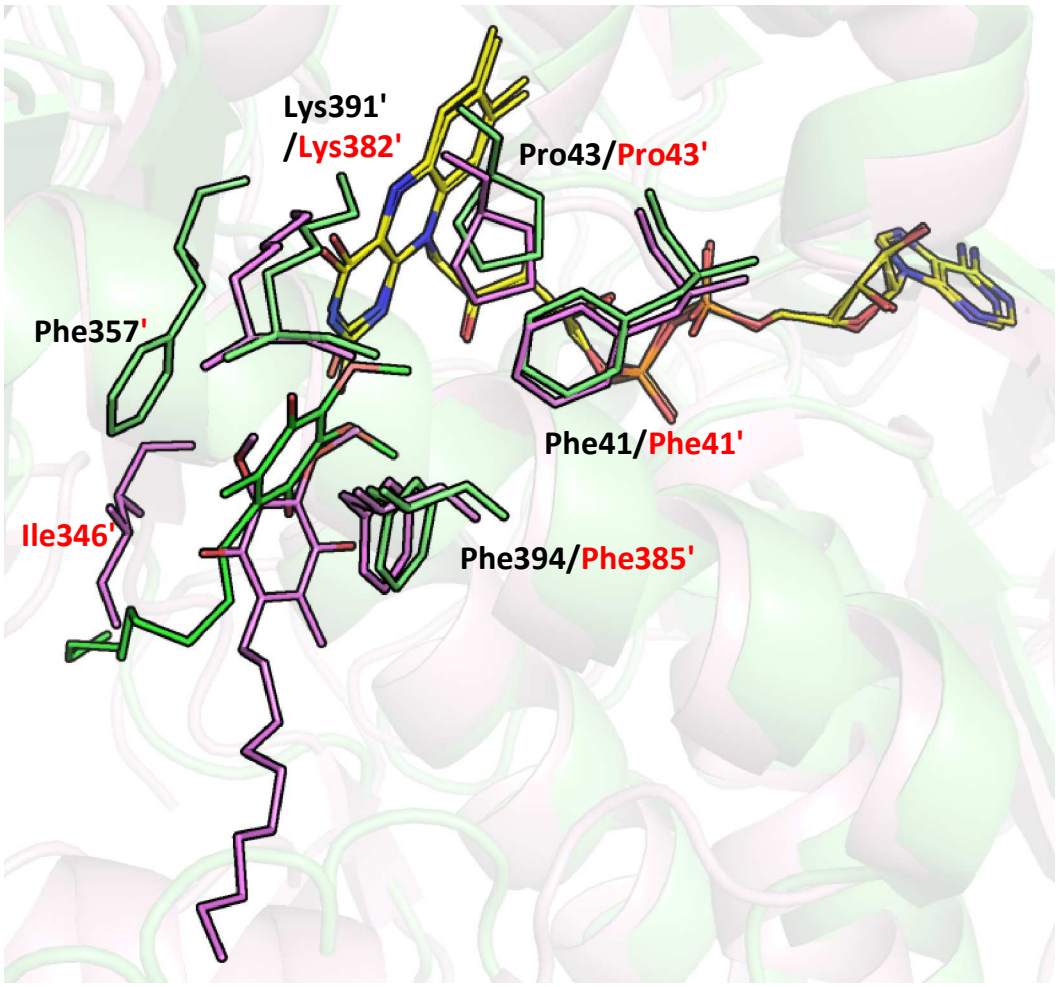
Lys391'
/Lys382'
Pro43/Pro43'
Phe357'
Phe41/Phe41'
Ile346'
Phe394/Phe385'